

Supplementary Information

**Ultrafast colorimetric humidity-sensitive polyelectrolyte coating for touchless control†**

Li Yu,<sup>a</sup> Haolan Xu,<sup>a</sup> Tanya M. Monroe,<sup>b</sup> David G. Lancaster,<sup>b</sup> Yi Xie,<sup>c</sup> Hongbo Zeng,<sup>d</sup>  
George Y. Chen\*<sup>b</sup> and Xiaokong Liu\*<sup>a</sup>

<sup>a</sup> Future Industries Institute, University of South Australia, Mawson Lakes, South Australia 5095, Australia

<sup>b</sup> Laser Physics and Photonic Devices Laboratories, School of Engineering, University of South Australia, Mawson Lakes, South Australia 5095, Australia

<sup>c</sup> Hefei National Laboratory for Physical Sciences at the Microscale, University of Science and Technology of China, Hefei, Anhui, 230026, P. R. China

<sup>d</sup> Department of Chemical and Materials Engineering, University of Alberta, Edmonton, Alberta, T6G 2V4, Canada

Address correspondence to George Y. Chen and Xiaokong Liu

Email: [george.chen@unisa.edu.au](mailto:george.chen@unisa.edu.au)

[xiaokong.liu@unisa.edu.au](mailto:xiaokong.liu@unisa.edu.au) or [liuxiaokong@gmail.com](mailto:liuxiaokong@gmail.com)

1. Supplementary Notes.
2. Supplementary Figures and Tables: Fig. S1- Fig. S28, Tab. S1
3. Supplementary References
4. Supplementary Movies: Movie S1-S8

## **1. Supplementary Notes**

### **1.1 Currently available touchless control technologies**

Currently, the dominant touchless control technology is based on speech recognition.<sup>S1,S2</sup> However, the accuracy of speech recognition is restricted by ambient noise, the ease of being overheard weakens the security, and it is unsuitable for voice-impaired users or noisy environments. Gesture-recognition-based touchless control<sup>S3,S4</sup> is incompatible with physically impaired users, and offers weak security due to access by unintentional gestures. Capacitive-sensing-based touchless control<sup>S5,S6</sup> employed by handheld devices exhibits limited access range (*i.e.*, several mm), and also can be unsuitable for physically impaired users.

### **1.2 Theoretical explanation of the color display of the PDDA/PSS coating**

The color of a coating is a visible embodiment of its reflected light in the visible spectrum, which is determined by three factors, namely interference, optical loss and dispersion. Interference is a phenomenon arising from the combination of incident light reflected by the upper and lower boundaries of a thin-film coating. Owing to interference, the reflection by the coating is strengthened at certain wavelengths but weakened at others, resulting in an observable color. Optical loss describes the attenuation of light when propagating through the coating, which is resulted from the absorption of light by the materials of the coating. If the materials (*e.g.*, dyes) of the coating absorb light at specific wavelengths, it will reflect the light with complementary wavelength, which also induces a color display. Chromatic dispersion spatially separates the different wavelengths of a reflectance spectrum, breaking down its color into different components like a rainbow.

In reality, a light source emits light in a variety of directions. Nevertheless, only the rays of light at an incident angle mirroring the observation angle relative to the coating surface matter to the color display of the coating.

For the case of our PDDA/PSS coatings, both optical loss and dispersion do not contribute to their color display, while it is solely decided by interference, which will be discussed in detail below.

The reflectance spectrum of a coating can be modelled by plotting the power of its reflected light at each wavelength. The power of the reflected light at a specific wavelength can be predicted by Equation (S1) below, which takes interference, and optical loss into

account. As shown in Scheme S1, a group of rays strike the air-coating interface from a specific angle, with a fraction reflected and the rest refracted. The refracted portion experiences optical loss as it propagates through the medium. The second reflection at the coating-substrate interface returns a fraction of the remaining light back, where it interferes (*i.e.*, coherently combines) with the light of the first reflection. As a result of the two effects, the optical power ( $P$ ) at each wavelength ( $\lambda$ ) is a function of the initial optical power ( $P_0$ ), reflectivity (*i.e.*, Fresnel reflection coefficient) of the air-coating interface ( $R_1$ ) and coating-substrate interface ( $R_2$ ), the refractive index of the coating ( $n_2$ ), the single-pass optical loss of the coating ( $\alpha$ ), and the effective thickness ( $L$ ) seen by light<sup>S7</sup>:

$$P = P_0 \cdot \left[ \frac{(1 - R_1\alpha)^2 \cdot (1 - R_2\alpha)^2}{(1 - R_1R_2\alpha^2)^2 + 4\sqrt{R_1R_2}\alpha \sin^2\left(\frac{2\pi \cdot n_2L}{\lambda}\right)} \right] \quad (\text{S1})$$

where the effective thickness ( $L$ ) can be expressed in terms of the actual thickness ( $h$ ) and the refraction angle ( $\theta_r$ ):

$$L = \frac{h}{\cos \theta_r} \quad (\text{S2})$$

based on Snell's Law, the refraction angle is a function of the incident angle ( $\theta_i$ ) and the refractive index of air ( $n_1$ ) and coating ( $n_2$ ), which is wavelength-dependent:

$$\theta_r = \sin^{-1}\left(\frac{n_1}{n_2 \sin \theta_i}\right) \quad (\text{S3})$$

the Fresnel reflection coefficients are calculated from the average of its two polarization states, being parallel ( $R_{1\parallel}$ ,  $R_{2\parallel}$ ) and perpendicular ( $R_{1\perp}$ ,  $R_{2\perp}$ ) to the plane of the coating:

$$R_1 = \frac{R_{1\parallel} + R_{1\perp}}{2} \quad (\text{S4})$$

$$R_2 = \frac{R_{2\parallel} + R_{2\perp}}{2} \quad (\text{S5})$$

where both components<sup>S8</sup> are dependent on the refractive indices of air, coating and silicon ( $n_3$ ) that is wavelength-dependent, as well as  $\theta_i$ :

$$R_{1\parallel} = \left| \frac{n_1 \cdot \sqrt{1 - n_1^2/n_2^2 \cdot \sin^2 \theta_i} - n_2 \cos \theta_i}{n_1 \cdot \sqrt{1 - n_1^2/n_2^2 \cdot \sin^2 \theta_i} + n_2 \cos \theta_i} \right|^2 \quad (\text{S6})$$

$$R_{1\perp} = \left| \frac{n_2 \cdot \sqrt{1 - n_1^2/n_2^2 \cdot \sin^2 \theta_i} - n_1 \cos \theta_i}{n_2 \cdot \sqrt{1 - n_1^2/n_2^2 \cdot \sin^2 \theta_i} + n_1 \cos \theta_i} \right|^2 \quad (\text{S7})$$

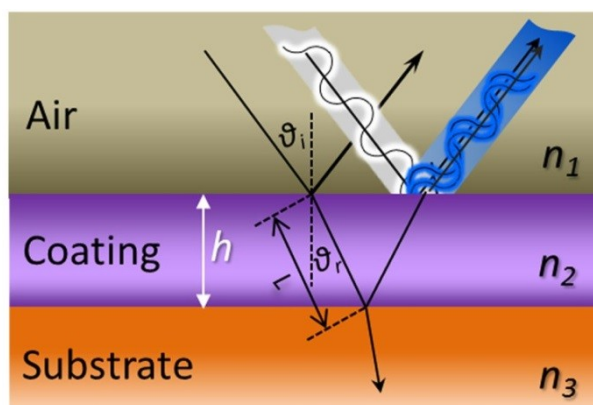
$$R_{2\parallel} = \left| \frac{n_2 \cdot \sqrt{1 - n_2^2/n_3^2 \cdot \sin^2 \theta_i} - n_3 \cos \theta_i}{n_2 \cdot \sqrt{1 - n_2^2/n_3^2 \cdot \sin^2 \theta_i} + n_3 \cos \theta_i} \right|^2 \quad (\text{S8})$$

$$R_{2\perp} = \left| \frac{n_3 \cdot \sqrt{1 - n_2^2/n_3^2 \cdot \sin^2 \theta_i} - n_2 \cos \theta_i}{n_3 \cdot \sqrt{1 - n_2^2/n_3^2 \cdot \sin^2 \theta_i} + n_2 \cos \theta_i} \right|^2 \quad (\text{S9})$$

Note that a complex component<sup>S9</sup> must be added to the refractive index of  $n_2$  and  $n_3$  to model imperfect reflections with lossy media. This takes into account the loss coefficient per unit length (*i.e.*, base e) of the material ( $\alpha_2, \alpha_3$ )

$$n_2 = n_{2,real} + j \cdot \frac{\lambda \alpha_2}{4\pi} \quad (\text{S10})$$

$$n_3 = n_{3,real} + j \cdot \frac{\lambda \alpha_3}{4\pi} \quad (\text{S11})$$



**Scheme S1** Schematic of the interference of light at the air-coating interface.

### 1.2.1 Optical loss of the PDDA/PSS coating

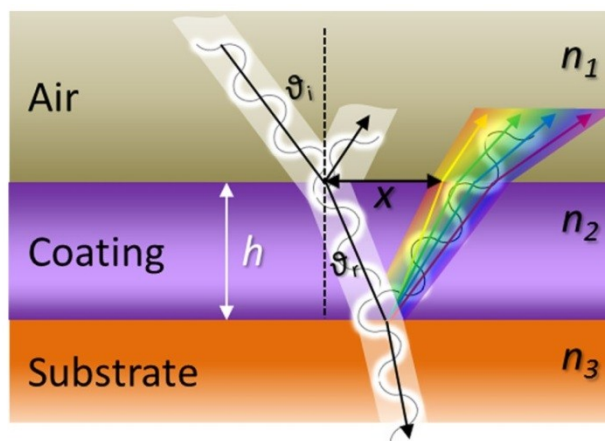
Fig. S1 shows the transmission and absorption spectra of the (PDDA/PSS)<sub>8.0</sub> coating prepared on a glass or quartz slide, respectively. It was found that the (PDDA/PSS)<sub>8.0</sub> coating does not show selective absorption of light (*i.e.*, equal optical loss) in the visible spectrum light (~350-800 nm), suggesting wavelength-independency for visible light. Accordingly, the optical loss does not contribute to the color display of the PDDA/PSS coating.

### 1.2.2 Chromatic dispersion of the PDDA/PSS coating

As shown in Scheme S2, though a group of rays strike the coating at the same spot, the internally reflected light emerges from the coating at different locations depending on the wavelength-dependent refractive indices. However, the reflectance spectrum is still the same if all the rays are captured. This displacement can be expressed in terms of  $h$  and  $\theta_r$ :

$$x = 2h \tan \theta_r \quad (\text{S12})$$

For the PDDA/PSS coating with thickness ( $h$ ) of several hundreds of nanometres, the displacements are too small to be resolved by the naked eye and most photodetectors. Therefore, the displacement effect (*i.e.*, dispersion) does not alter the color of the PDDA/PSS coatings.



**Scheme S2** Schematic of the dispersion of light from the coating.

### 1.2.3 Deduction of the refractive indices of the PDDA/PSS coatings

The refractive indices of the PDDA/PSS coatings can be deduced by their known thickness as described below. The thickness of the PDDA/PSS coatings was measured by the Filmetrics instrument, which was also verified by stylus profilometer, which showed good agreement, as shown in Fig. S2 and S3. Although the Filmetrics instrument can also provide refractive index results, they were not easily verifiable and thus not used.

With the known thickness of a coating, its refractive index at a specific wavelength can be derived from knowing the period of the corresponding spectrum centred at that wavelength using Equation (S19) (see Part 1.4 of the Supplementary Notes).

The period ( $\Delta\lambda$ ) at a specific wavelength can be calculated from the reflectance spectrum with the knowledge of two pairs of peak ( $L_1, L_2$ ) and valley ( $L_3, L_4$ ) wavelengths:

$$\Delta\lambda = \frac{2 \times [(L_4 - L_3) - (L_2 - L_1)]}{\frac{L_4 + L_3}{2} - \frac{L_2 + L_1}{2}} \cdot \left[ \lambda - \frac{L_2 + L_1}{2} \right] + 2 \times (L_2 - L_1) \quad (\text{S13})$$

This equation works by first finding two half-periods in the reflectance spectrum, and the corresponding center wavelengths. Then, the period for a given wavelength ( $\lambda$ ) can be interpolated from the position of that center wavelength with respect to the other two center wavelengths, as expressed by the Equation (S13). An example is shown in Fig. S4. To

accurately calculate the periods, it is important that the optical loss is fairly wavelength-independent, which has been verified to be true for the case of our PDDA/PSS coatings in Fig. S1.

#### 1.2.4 Modelling the reflectance spectrum of the PDDA/PSS coating

Knowing the thickness, refractive index and optical loss of a coating, its reflectance spectrum can be modelled using Equation (S1) with a high degree of accuracy. As an example, Equation (S1) is used to simulate the reflectance spectrum of the (PDDA/PSS)<sub>8.0</sub> coating at a RH of 58% (shown in Fig. S5), observed at the normal to the coating surface. It can be seen that there is an excellent agreement between the periods of the simulated and measured spectra.

#### 1.3 Effect of substrate

The optical characteristics of the substrate also play an important role on the color display of the PDDA/PSS coatings. The color of the PDDA/PSS coating is best observed when a partially reflective, absorbing/opaque and colourless substrate is used. A low-reflectivity substrate does not provide the degree of second interface reflection needed for a strong interference visibility. Although a high-reflectivity substrate generates a strong reflection by the second interface needed for a strong interference visibility, it may also flatten the reflectance spectrum. An absorbing/opaque substrate prevents light behind it to shine through, which may dominate the color display. A colourless substrate with a flat reflectance across the visible spectrum maximizes the range of displayed colors. Theoretically, the most efficient interference occurs when the reflectivity of the air-coating interface matches that of the coating-substrate interface. Based on the Fresnel equation, for the case of normal incidence, the required refractive index at a specific wavelength of the substrate can be solved from the quadratic expression of Equation (S14):

$$\left(\frac{n_2 - n_3}{n_2 + n_3}\right)^2 = \left(\frac{n_1 - n_2}{n_1 + n_2}\right)^2 \quad (\text{S14})$$

where  $n_1$ ,  $n_2$  and  $n_3$  are the refractive indices of air, coating and substrate, respectively. Accordingly,  $n_3$  is calculated to be 1.82 at 633 nm by setting  $n_1$  and  $n_2$  to be 1 and 1.35 (see Fig. S14), respectively. In reality, there is always an optical loss when light propagates through a coating, which decreases the power of the reflected light at the coating-substrate interface. Therefore, a substrate with a substantially higher refractive index is required. One

of the most promising candidates is silicon, which has refractive indices greater than 3.7 in the visible spectrum. More importantly, it is widely available at a low cost.

#### 1.4 Relationship between the center wavelength and its corresponding period

In a sinusoidal reflectance spectrum, by considering the difference in wavelength to produce a phase difference of  $2\pi$ , Equation (S19) can be sequentially derived from Equation (S15). It reveals that the wavelength-dependent period is inversely proportional to  $h$ , and thus more fringes can be observed in a fixed wavelength range if the coating is thicker. We begin with the well-known phase ( $\varphi$ ) expression of light as an electromagnetic wave:

$$\varphi = \frac{2\pi}{\lambda} \cdot n_2 h \quad (\text{S15})$$

Choosing two arbitrary wavelengths ( $\lambda_1$  and  $\lambda_2$ ) to produce a phase difference of  $2\pi$ , or one phase cycle, or one period:

$$2\pi = \left( \frac{4\pi}{\lambda_1} - \frac{4\pi}{\lambda_2} \right) \cdot n_2 h \quad (\text{S16})$$

Rearranging Equation (S16):

$$\frac{\lambda_1 - \lambda_2}{\lambda_1 \lambda_2} = \frac{1}{2n_2 h} \quad (\text{S17})$$

Approximating the product of the two similar wavelengths as the product of their center wavelength ( $\lambda$ ):

$$\frac{\Delta\lambda}{\lambda^2} = \frac{1}{2n_2 h} \quad (\text{S18})$$

Finally, rearranging once more gives:

$$\Delta\lambda = \frac{\lambda^2}{2n_2 h} \quad (\text{S19})$$

#### 1.5 Relationship between the coating thickness and its peak position

For light reflecting within a thin-film coating, the phase delay of a roundtrip (*i.e.* two passes) must equal an integer ( $m$ ) multiple of  $2\pi$  for the reflection to experience constructive interference. As a result, the peak wavelength ( $\lambda_p$ ) is governed by Equation (S21) that is derived from Equation (S20):

$$\frac{4\pi}{\lambda_p} \cdot n_2 h = 2\pi m \quad (\text{S20})$$

$$\lambda_p = \frac{2n_2 h}{m} \quad (\text{S21})$$

### **1.6 Working principle of the comparator circuit used in the touchless control system**

The comparator circuit<sup>S10</sup> shown in Fig. 4c in the main article of the manuscript consists of an operational amplifier with two inputs, one for the signal voltage and one for the reference voltage. If the signal voltage exceeds the reference voltage, the output is rapidly pulled up to the supply voltage, otherwise it remains at the ground voltage. The feedback resistors facilitate the hysteresis function to suppress noise-induced switching. The ratio of the resistors governs the lower and upper thresholds for switching the output between low and high levels.

## 2. Supplementary Figures and Tables

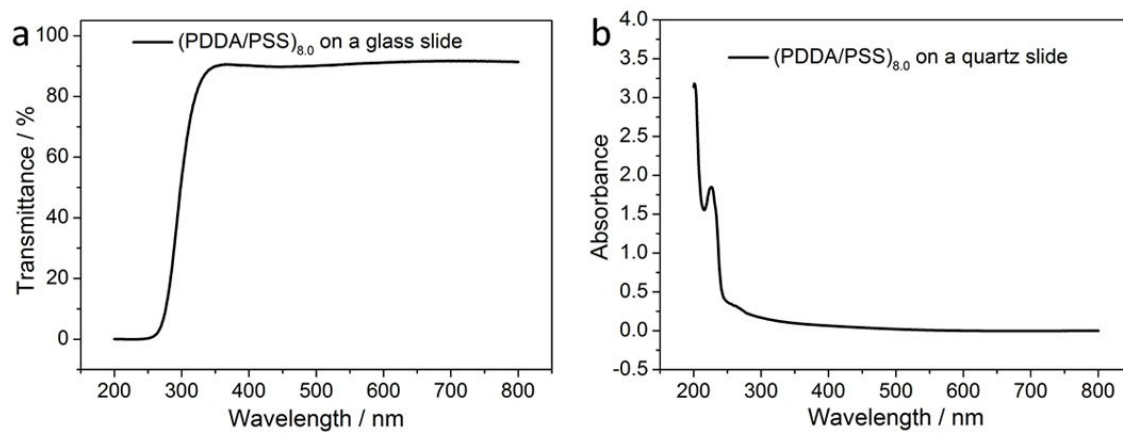


**Fig. S1** Transmission (a) and absorption (b) spectra of the (PDDA/PSS)<sub>8.0</sub> coating overlaid on a glass (a) or quartz (b) slide in the UV-visible spectrum.

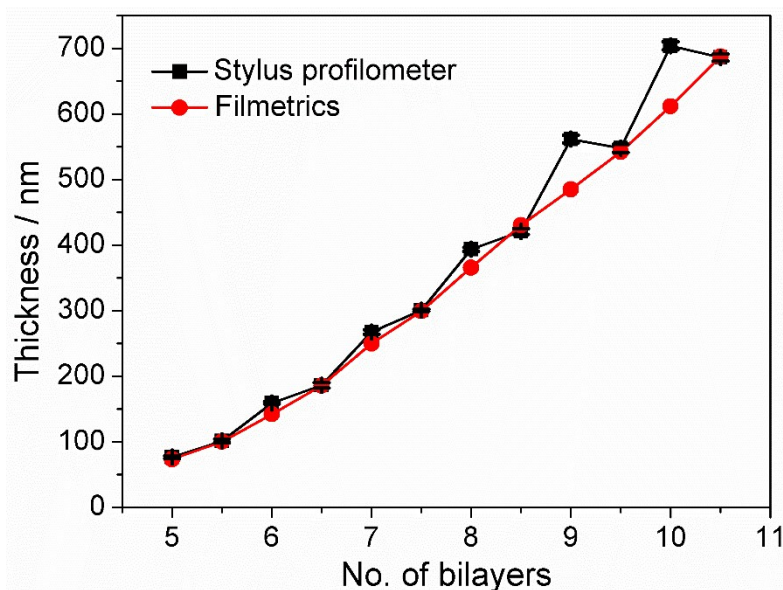


**Fig. S2** Comparison of the thickness of the  $(\text{PDDA}/\text{PSS})_N$  coatings, measured by a Filmetrics and a stylus profilometer instruments at the ambient RH.

As shown in this figure, the thickness results measured by the Filmetrics instrument and the Stylus profilometer show near-exact agreement for the coatings with half bilayers (*i.e.*, PDDA as the outmost layer). In contrast, increasing thickness difference is observed with increasing bilayer numbers for the coatings with whole bilayers (*i.e.*, PSS as the outmost layer). This phenomenon can be well explained by the surface morphology of the  $(\text{PDDA}/\text{PSS})_N$  coatings, and the different mechanisms of the two characterization methods. As shown in Fig. S3, the surface roughness/morphology of the  $(\text{PDDA}/\text{PSS})_N$  coatings is zigzagged when their outmost layer switches between PDDA and PSS. The PDDA-capped coatings are very smooth with a surface roughness ( $R_q$ ) typically lower than 10 nm for the measured coatings. On the contrary, the PSS-capped coatings show relatively high surface-roughness, which significantly increases with increasing the bilayer numbers. The Filmetrics instrument is an optical technique that measures thickness, which considers the distance travelled by light. Therefore, for a rough surface, the height of the surface features is accurately averaged to generate the thickness reading. Differently, the stylus profilometer physically measures the coating thickness by tracing the profile of a moving stylus across a scratched coating, where the height difference between the intact coating and the exposed substrate (*i.e.*, in the scratch) yields the coating thickness. Although the profilometer takes the average height of the surface features, its sampling/averaging resolution is decided by the coating roughness, the size of the stylus, and the accuracy of the motorized translation stage. For surfaces with high roughness at nanoscale, it is rather difficult to follow the surface features with the stylus. Hence, it is reasonable to assume that the stylus profilometer provides higher thickness readings for a rough surface compared to the Filmetrics instrument.

Nevertheless, after comparing the thickness results provided by the Filmetrics instrument and the stylus profilometer, one can conclude that the thickness data produced from the Filmetrics measurements are accurate.

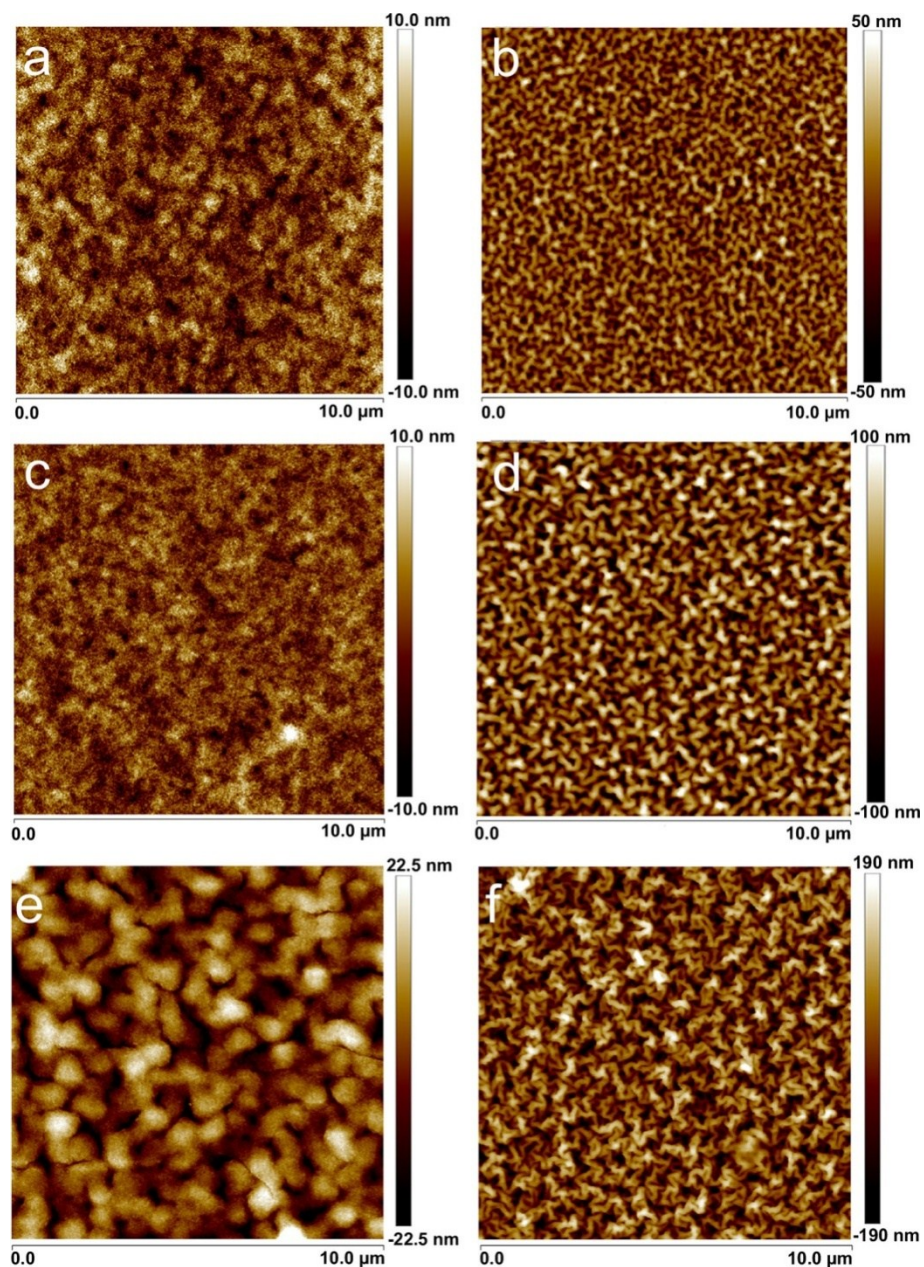


**Fig. S3** (a-f) AFM images ( $10 \times 10 \mu\text{m}^2$  area) of the  $(\text{PDDA}/\text{PSS})_N$  coatings with  $N$  of 5.5 (a), 6 (b), 7.5 (c), 8 (d), 8.5 (e), 9 (f). The root-mean-square roughness ( $R_q$ ) of the coatings shown in (a-f) is 2.49 (a), 14.4 (b), 2.98 (c), 41.1 (d), 8.49 (e) and 71.2 (f) nm, respectively. This figure is used to support the discussion of Fig. S2.

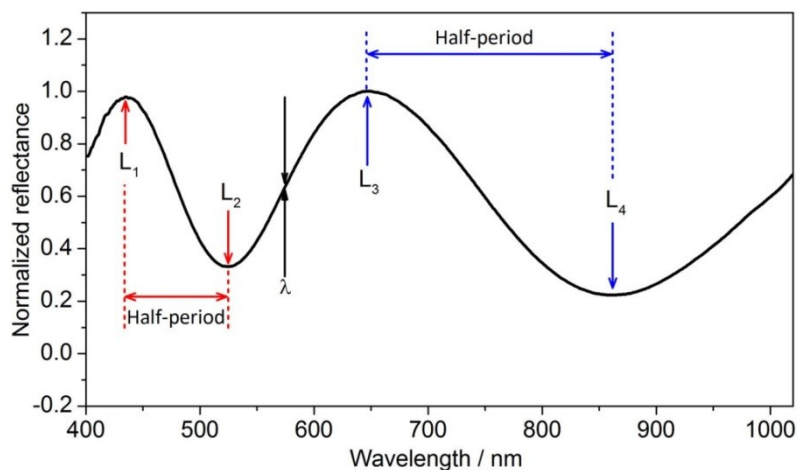


**Fig. S4** Illustration of how to calculate the period centred at a particular wavelength ( $\lambda$ ) using Equation (S13).

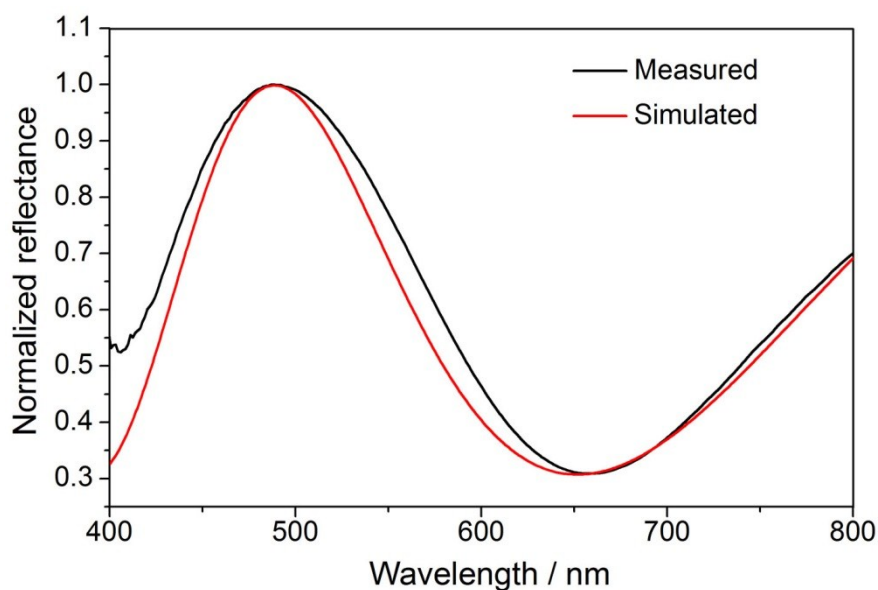


**Fig. S5** Comparison of the reflectance spectrum of the  $(\text{PDDA/PSS})_{8.0}$  coating at a RH of 58%, between the measured data using the Filmetrics instrument (black curve), and the simulated data using Equation (S1) (red curve). The view angle is set as normal to the sample.



**Fig. S6** Photographs the  $(\text{PDDA/PSS})_N$  coatings with  $N$  varying from 11.0 to 15.0, taken at a viewing angle perpendicular to the coating surface. Half and whole bilayers denote coatings with PDDA and PSS as the outmost layer, respectively.

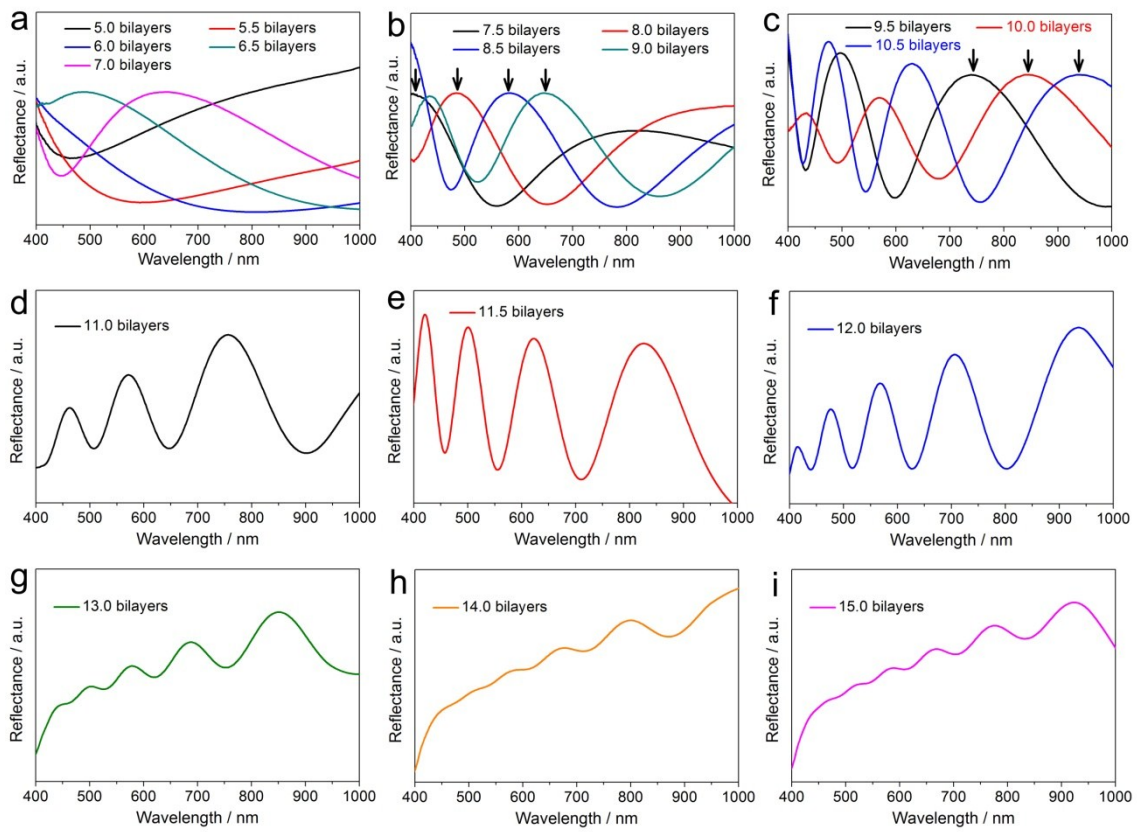


**Fig. S7** Reflectance spectra of the  $(\text{PDDA/PSS})_N$  coatings across the wavelengths range between 400 nm and 1000 nm, with  $N$  varying from 5.0 to 15.0. The arrows shown in (b) and (c) indicate the nominated reflection peaks that are tracked.

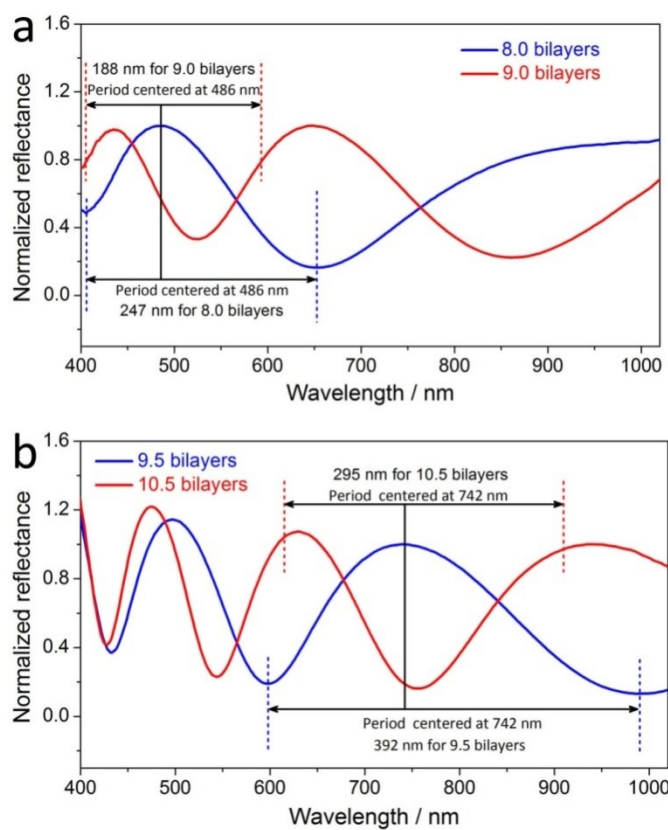


**Fig. S8** Period comparison between the reflectance spectrum of different (PDDA/PSS)<sub>N</sub> coatings. The period of the pattern at a specific wavelength is found by tracing sideways at equal spacing from the specific wavelength.

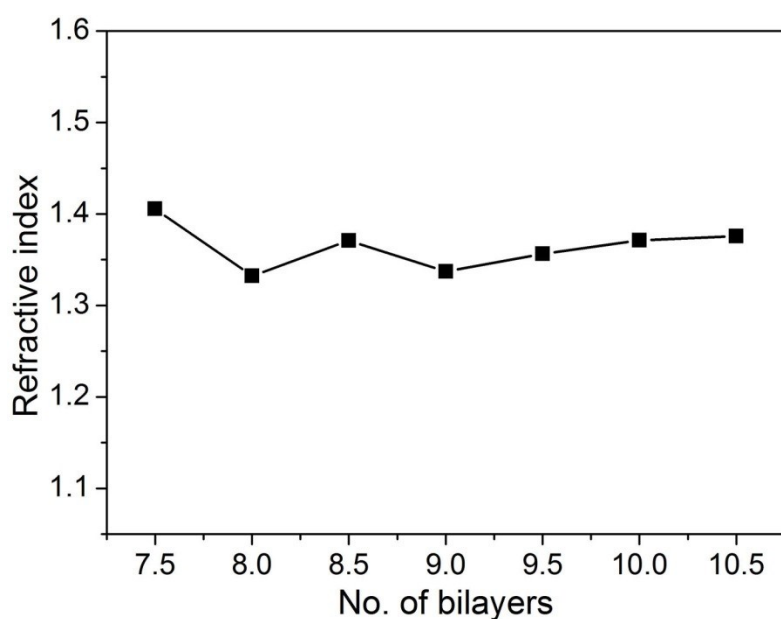


**Fig. S9** Refractive indices at 633 nm wavelength of the (PDDA/PSS)<sub>N</sub> coatings as a function of the bilayer number (*N*).

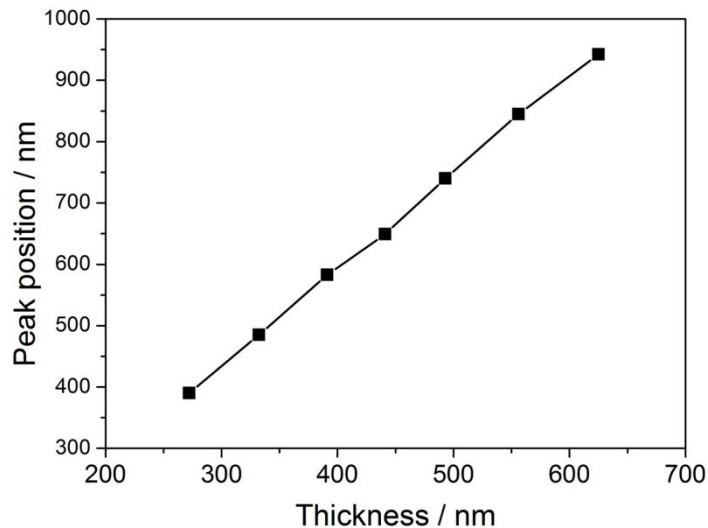


**Fig. S10** Relationship between the peak position and thickness of the (PDDA/PSS)<sub>N</sub> coatings with *N* varying from 7.5 to 10.5. The peak position means the wavelength of the nominated peak in the corresponding reflectance spectra.



**Fig. S11** Photographs of the (PDDA/PSS)<sub>7.5</sub> coating under different RH varying from 0% to 100%

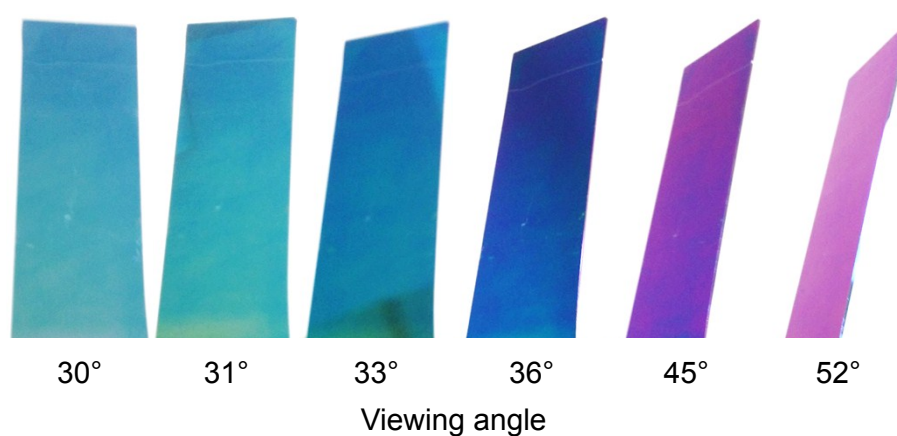


**Fig. S12** Photograph of the color evolution of the (PDDA/PSS)<sub>8.0</sub> coating, taken at various viewing angles relative to the normal incidence. Above 33° the color becomes significantly different.

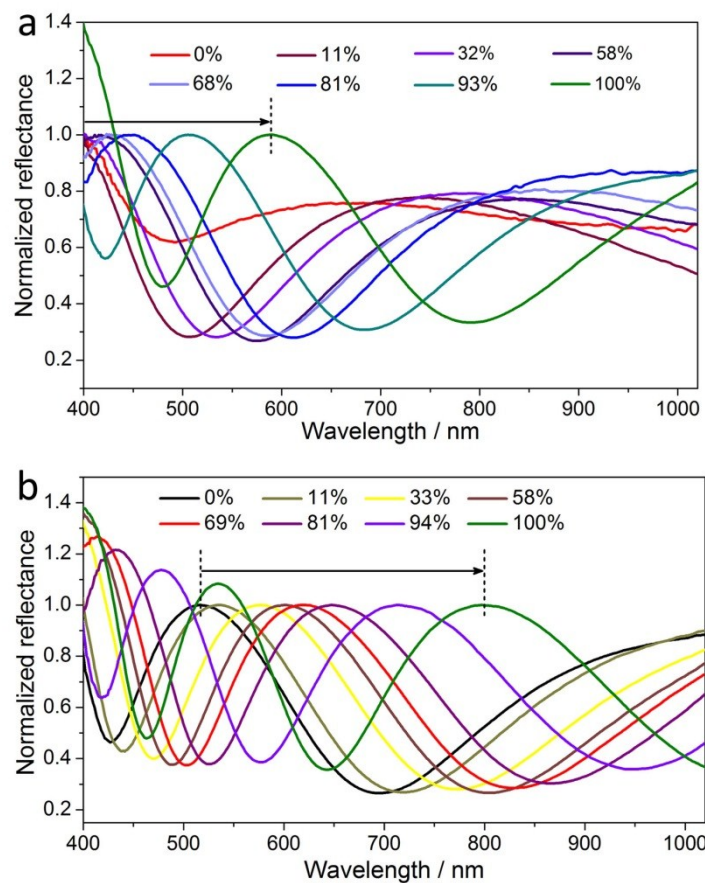


**Fig. S13** Reflectance spectra of the  $(\text{PDDA/PSS})_{7.5}$  (a) and  $(\text{PDDA/PSS})_{8.5}$  (b) coating across the wavelength range between 400 nm and 1020 nm at different RH varying from 0% to 100%.

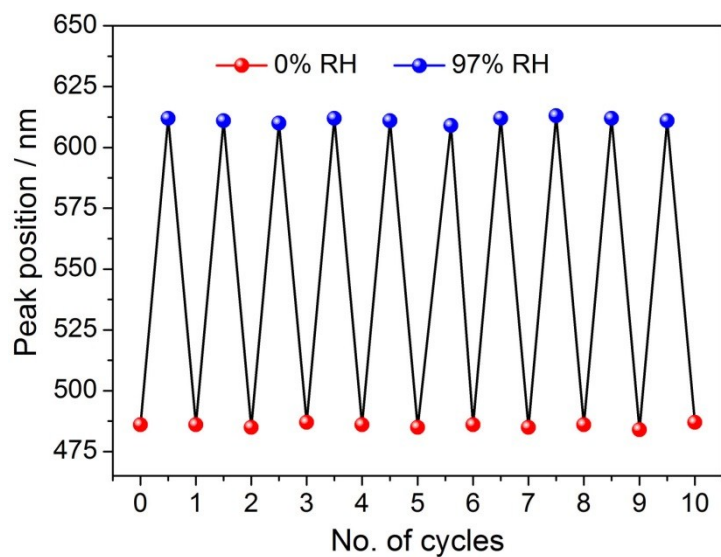


**Fig. S14** Recoverability of the nominal peak position in the reflectance spectrum of the (PDDA/PSS)<sub>8.0</sub> coating when the environmental RH was cycled between 0% and 97%.

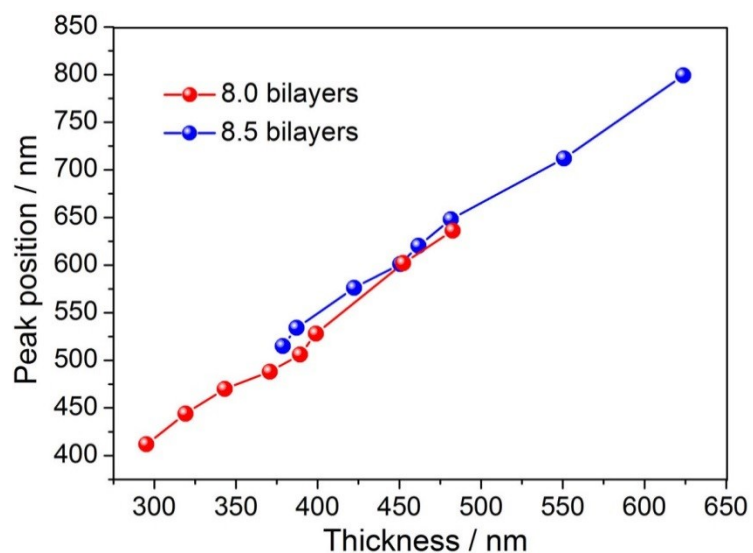


**Fig. S15** Relationship between the peak position in the reflectance spectrum and the thickness of the (PDDA/PSS)<sub>8.0</sub> (red dots) and (PDDA/PSS)<sub>8.5</sub> (blue dots) coatings at different RH (also see Fig. 2c and 2d in the main article).

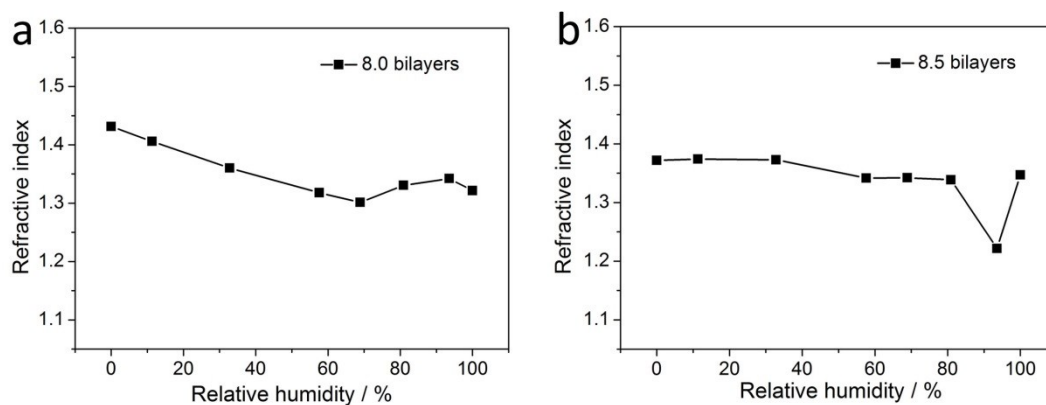


**Fig. S16** Refractive indices at 633 nm wavelength of the (PDDA/PSS)<sub>8.0</sub> (a) and (PDDA/PSS)<sub>8.5</sub> (b) coatings at RH varying from 0% to 100%.

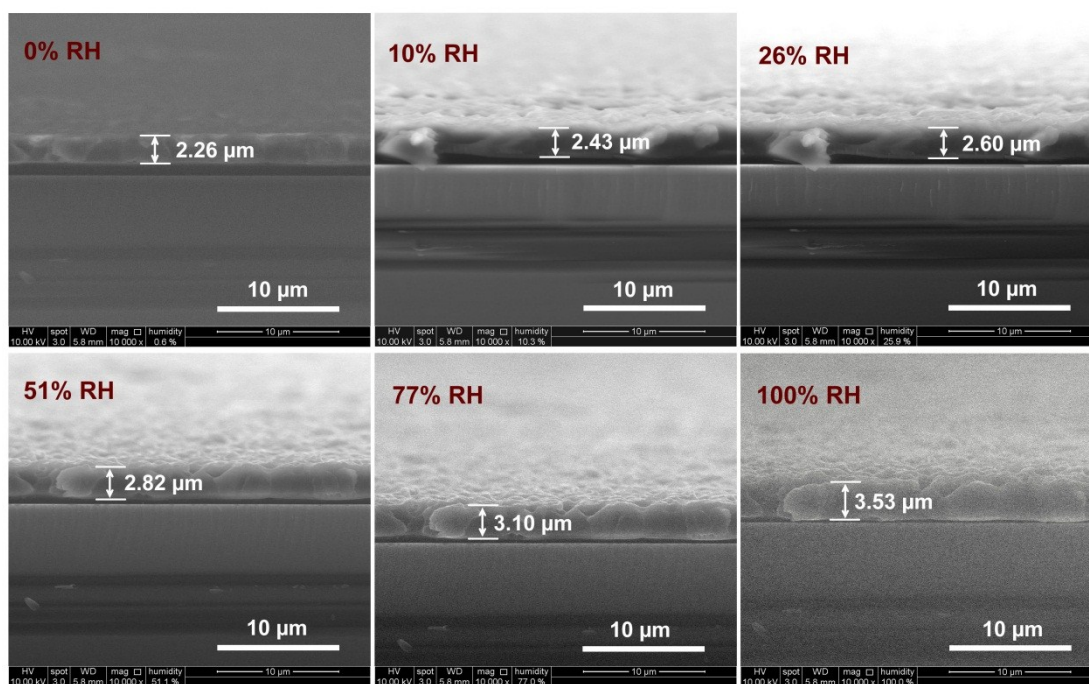


**Fig. S17** Cross-section ESEM images of the (PDDA/PSS)<sub>20</sub> coating measured at RH of 0%, 10%, 26%, 51%, 77% and 100%.

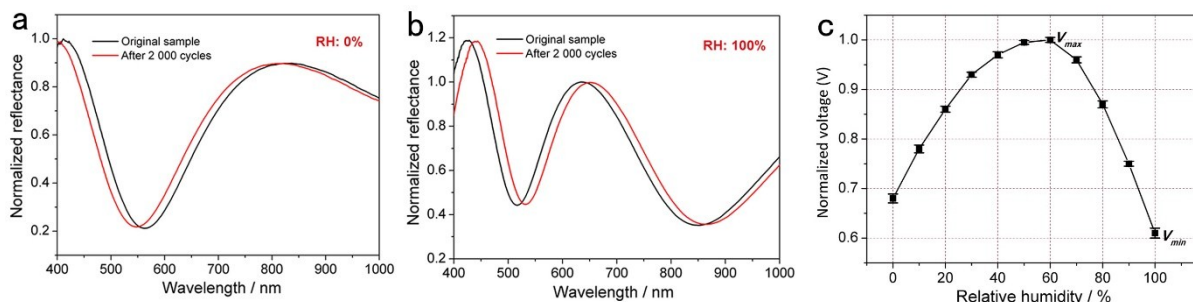


**Fig. S18** (a, b) Reflectance spectra of the (PDDA/PSS)<sub>8.0</sub> coating before (black curves) and after (red curves) being cyclically exposed to 100% and 0% RH for 2000 times, which were measured at RH of 0% (a) and 100% (b), respectively. (c) The normalized voltage of the electrical signals generated from the modulation of light by the as-treated (PDDA/PSS)<sub>8.0</sub> coating as a function of RH to which the sample was exposed. The method and setup that were used to generate the electrical signals based on the color change of the coatings at varied RH are described/shown in Part 3.3 and Fig. 3 in the main article of this paper.

After the cyclic exposure to 100% and 0% RH for 2000 times, the reflectance spectrum of the (PDDA/PSS)<sub>8.0</sub> coating at RH of 0% blue-shifted by 14 nm compared to that of the original sample, while that measured at RH of 100% red-shifted by 16 nm. Therefore, it can be concluded that the colorimetric humidity-sensitive property of the coating was still well kept and the RH-dependent peak-position shift was even enlarged after the treatment.

The response and recovery times of the 2000-cycle sample were measured to be ca. 38 ms and 980 ms, respectively. The new normalized voltage as a function of RH is plotted in Fig. S18c.  $V_{max}$  and  $V_{min}$  are now located at coordinates (60%RH, 1.00 V<sub>norm</sub>) and (100%RH, 0.61 V<sub>norm</sub>), respectively. The more significant change for  $V_{min}$  is due to the larger peak-position shift at very low and very high RH.

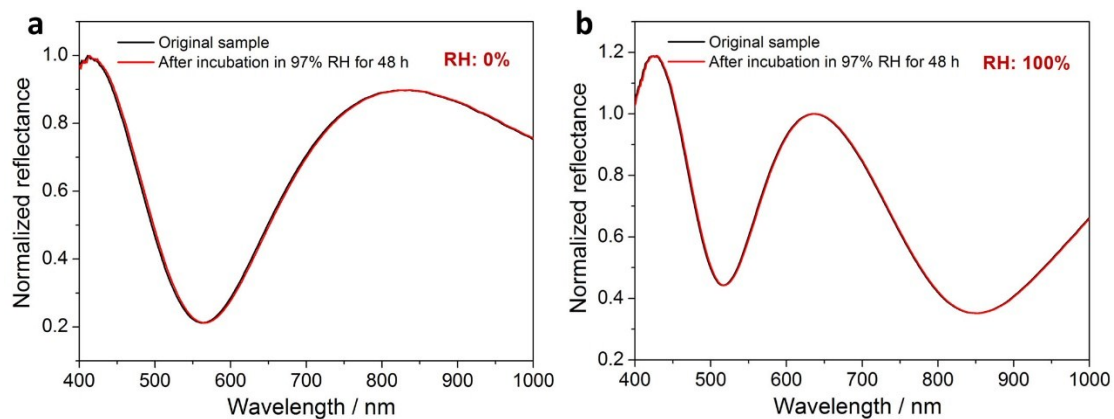


**Fig. S19** (a, b) Reflectance spectra of the (PDDA/PSS)<sub>8.0</sub> coating before (black curves) and after (red curves) being incubated in 97% RH for 48 h, which were measured at RH of 0% (a) and 100% (b), respectively.

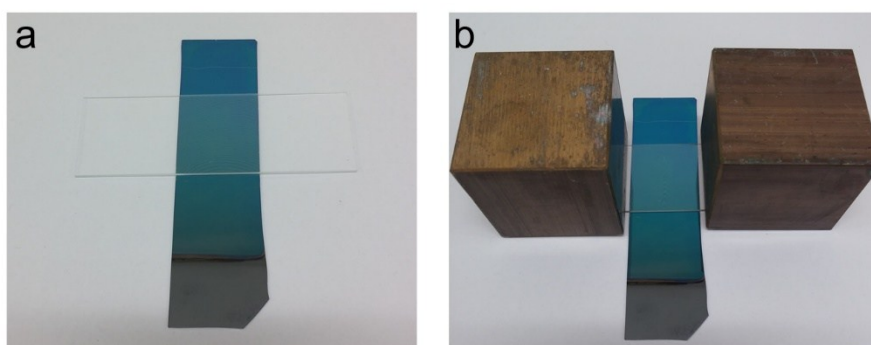


**Fig. S20** (a) Photograph of the (PDDA/PSS)<sub>8.0</sub> coating sample covered with a glass slide. (b) Photograph showing that two copper cubes with total weight of 1.0 kg was pressing down on the (PDDA/PSS)<sub>8.0</sub> coating separated by a glass slide. It can be observed that the coating under the pressure did not exhibit any color change.

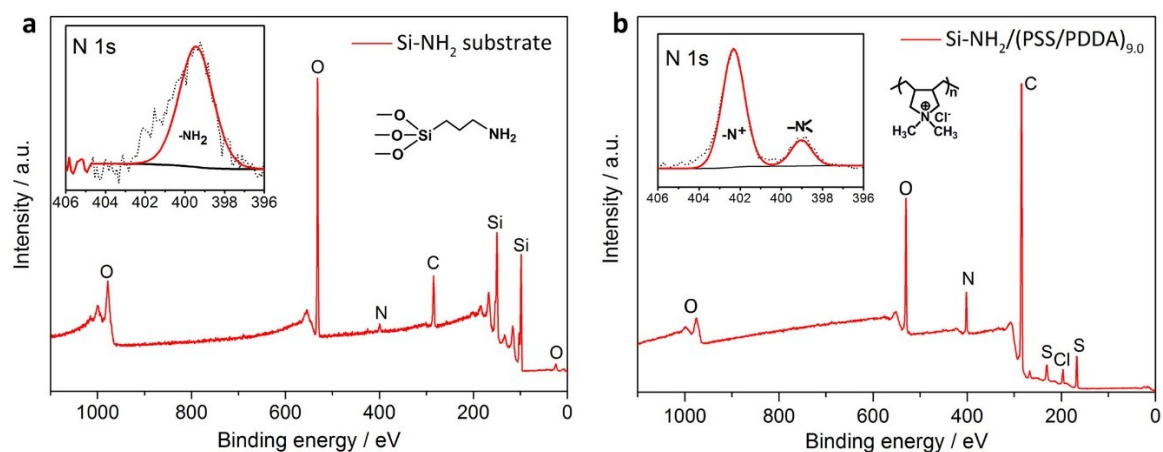


**Fig. S21** (a, b) XPS wide scan and high resolution (N element, insets) spectra of the Si-NH<sub>2</sub> substrate (a) and the (PSS/PDDA)<sub>9,0</sub> PEMs (with PDDA as the outmost layer) deposited on the Si-NH<sub>2</sub> substrate. The analysis of the high resolution XPS spectra of the N element in both samples verifies the modification of the Si substrate with amino groups and the deposition of the PSS/PDDA PEMs on the Si-NH<sub>2</sub> substrate, respectively.

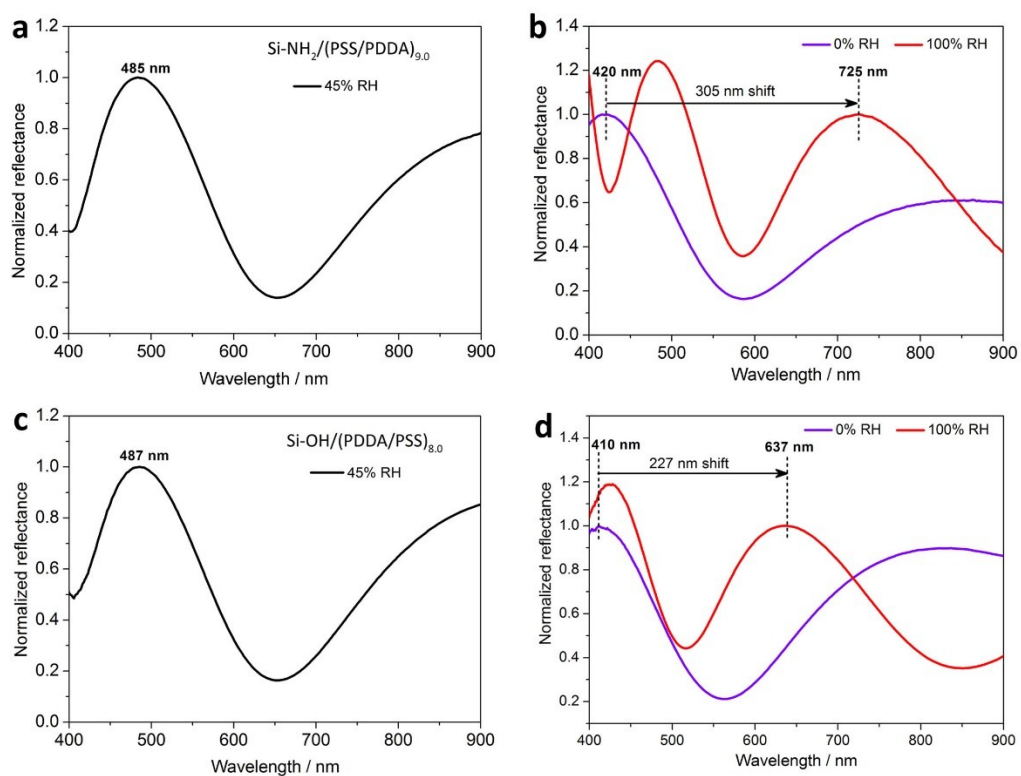


**Fig. S22** (a-d) Reflectance spectra of the  $\text{Si-NH}_2/(\text{PSS}/\text{PDDA})_{9.0}$  (a, b) and  $\text{Si-OH}/(\text{PDDA}/\text{PSS})_{8.0}$  (c, d) samples, measured at the ambient conditions (ca. 45% RH) (a, c), 0% RH (b, d, violet curves) and 100% RH (b, d, red curves).

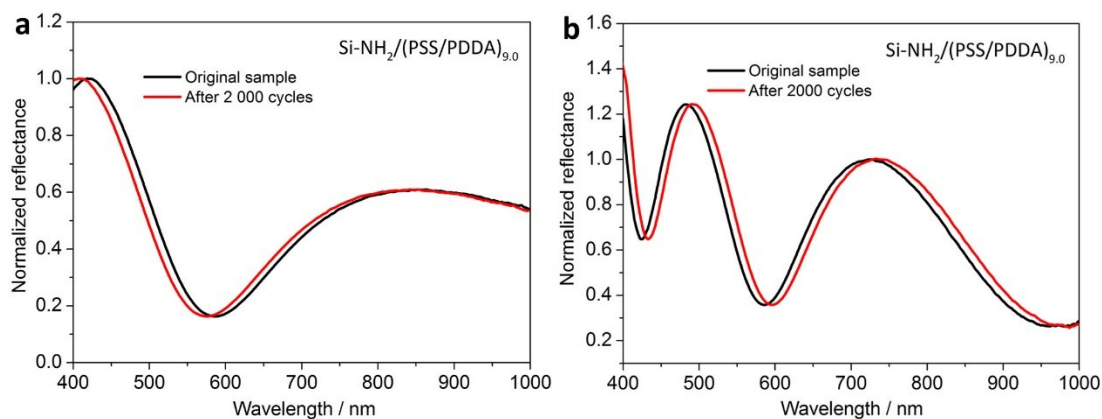


**Fig. S23** (a, b) Reflectance spectra of the Si-NH<sub>2</sub>/(PSS/PDDA)<sub>9,0</sub> sample before (black curves) and after (red curves) being cyclically exposed to 100% and 0% RH for 2000 times, which were measured at RHs of 0% (a) and 100% (b), respectively.

It can be found that, after the cyclic exposure to 100% RH and 0% RH for 2000 times, the reflectance spectrum of the Si-NH<sub>2</sub>/(PSS/PDDA)<sub>9,0</sub> sample at a RH of 0% blue shifted by 11 nm compared to that of the original sample, while that measured at a RH of 100% red shifted by 12 nm.

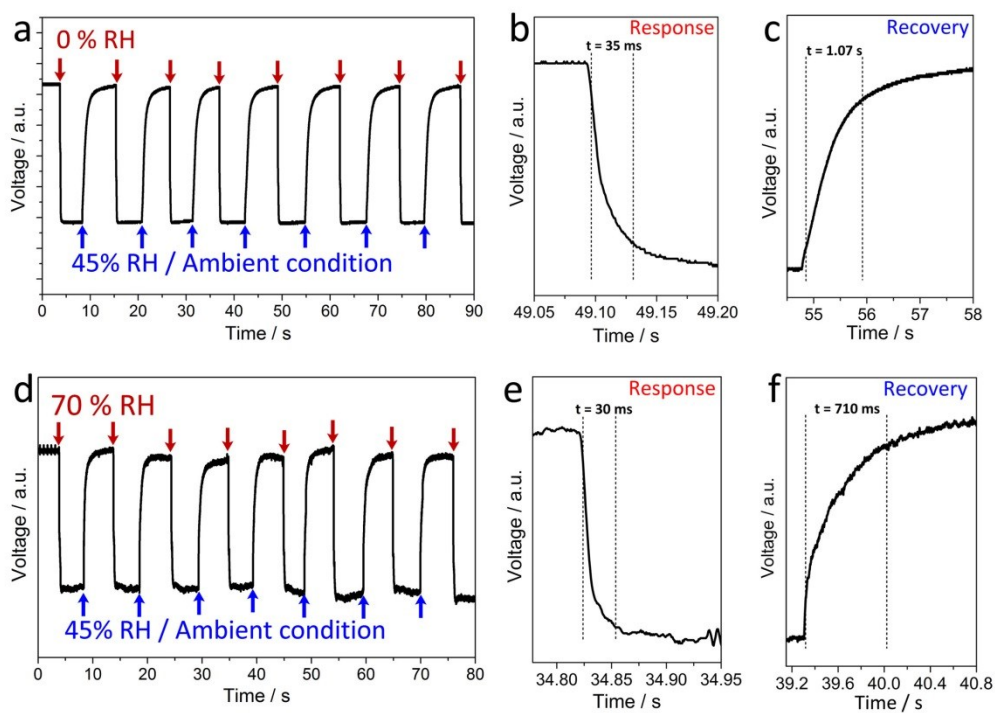


**Fig. S24** (a, d) Temporal response of the electrical signal generated from the modulation of light by the (PDDA/PSS)<sub>8.0</sub> coating while the RH exposed to the sample was switched between 45% and 0% (a) or 70% (d). (b, c) Enlarged view of (a) in the time ranges of 49.05 s to 49.20 s (b) and 54.5 s to 58 s (c). (e, f) Enlarged view of (d) in the time ranges of 34.78 s to 34.95 s (e) and 39.2 s to 40.8 s (f).

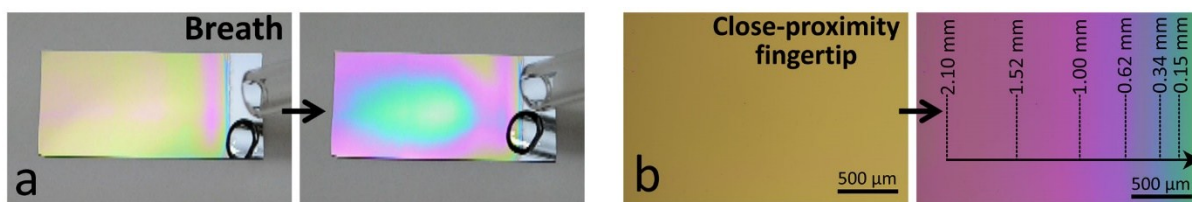


**Fig. S25** (a) Photographs of the (PDDA/PSS)<sub>8.5</sub> coating before and after a human breath was exhaled on its surface, with the breath guided by a glass tube. (b) Microscope image of the (PDDA/PSS)<sub>8.5</sub> coating before and after a finger was placed at c.a. 1 mm to the right side of the sample, the distance from the localized position on the sample to the finger is labelled on the image.

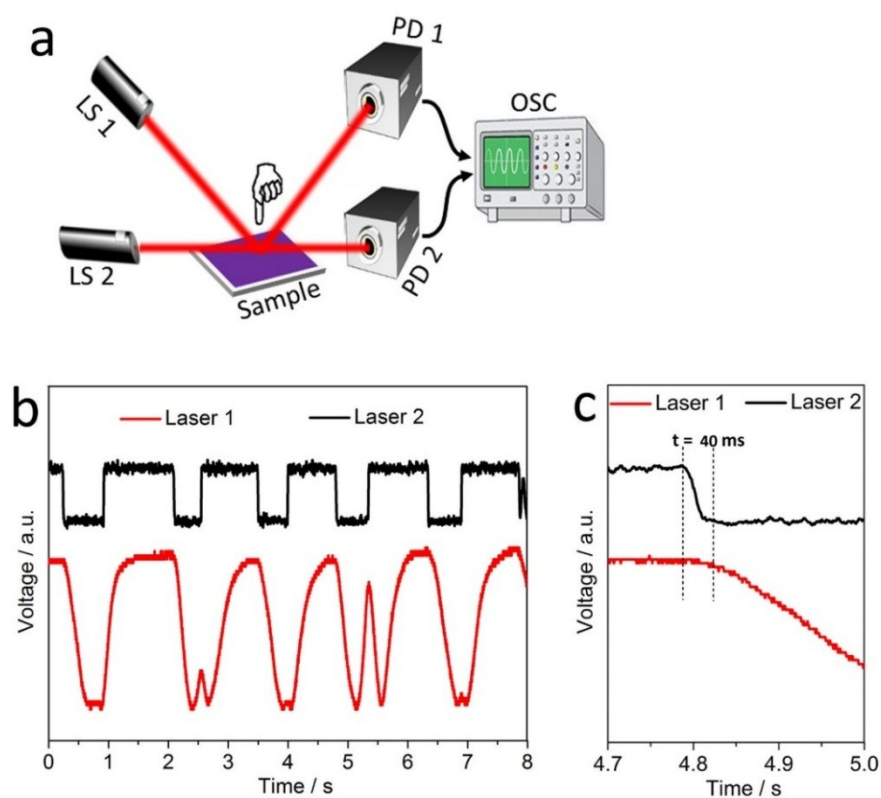


**Fig. S26** (a) Schematic of the experimental setup for the measurement of the reaction time of the (PDDA/PSS)<sub>8.0</sub> coating to a close-proximity fingertip. (b) Voltage response of the signals originated from LS 1 and LS 2 during the course of cyclic fingertip proximity towards the coating surface at a distance of 5 mm. (c) Enlarged view of (b) in the time range of 4.7 s to 5.0 s.

The first laser source (LS 1) is used to monitor the response of the coating to the proximate fingertip, the second laser source (LS 2) is used to detect the finger position. The distance between the LS 2 beam and the coating surface was set to 5 mm. If a finger approaches the coating surface, it will block the LS 2 beam at a distance of 5 mm. Therefore, the LS 2 signal displays a sharp drop on the oscilloscope, which indicates that the finger is in range of stimulating the coating, and should not move any closer. Subsequently, the moisture discharged from the finger reaches the coating and induces the coating to react. As a result, the optical signal from LS 1 is modulated and displayed on the oscilloscope. Lastly, the time taken for the coating to react when a fingertip is in close proximity is defined as the reaction time, calculated from the difference in signal change between the LS 1 and LS 2 signals.

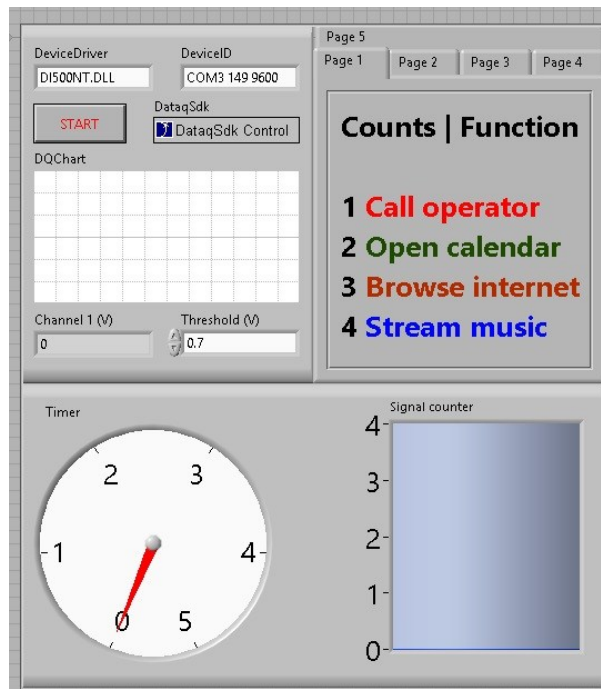


**Fig. S27** Block diagram of the Labview program for the touchless-control of a personal computer (PC).

The graphical user interface for the PC demonstration of touchless control was implemented using the *Labview* software. The functionality is essentially a comparator, counter and a timer working in union. This interface allows the user to input a voltage threshold, below which a command will be implemented. For every time the signal drops below the threshold voltage, the counter increments by 1, and the timer resets to zero. If there is inactivity (i.e. above threshold) for more than 5 seconds, the number of counts will be analysed and the corresponding command will be generated. Some of the commands involve opening a web browser or playing music, which requires the windows console-style script to be executed. For example, “cmd /c start http://www.abc.net.au”.

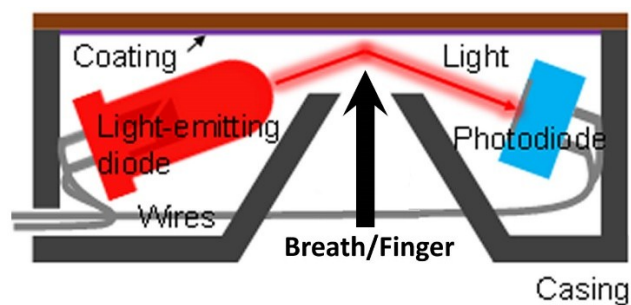


**Fig. S28.** Proposed schematic showing how a miniaturized device can be assembled using low-cost off-the-shelf components.

The device can be miniaturized by using an LED, photodiode and suitable packaging illustrated by the above schematic. The inward funnel in the casing allows moisture from the atmosphere/breath/finger to interact with the humidity-sensitive coating, while the beam of light interrogates the physical changes. The light-emitting diode and photodiode can be simply glued in place within the casing. The dimensions of the packaged device can be as small as  $1 \times 2 \times 4$  cm.

**Tab. S1.** List of the chemicals used for producing the different corresponding RH in a sealed cuvette. Saturated aqueous solutions of the salts (*i.e.*, 2-13) were used.

<b>Chemicals</b>	<b>RH (% , 25 °C)</b>
1. Silica gel	0
2. Lithium chloride	11.30
3. Potassium acetate	22.51
4. Magnesium chloride	32.78
5. Potassium carbonate	43.16
6. Magnesium nitrate	52.89
7. Sodium bromide	57.57
8. Potassium iodide	68.86
9. Sodium chloride	75.29
10. Potassium bromide	80.89
11. Potassium chloride	85.06
12. Potassium nitrate	93.58
13. Potassium sulphate	97.30
14. Pure water	100

### 3. Supplementary References

- [S1] D. Kang, P. V. Pikhitsa, Y. W. Choi, C. Lee, S. S. Shin, L. Piao, B. Park, K.-Y. Suh, T. Kim and M. Choi, *Nature*, 2014, **516**, 222-226.
- [S2] S. Kim and Speech Recognition. U.S. Patent 9251804 B2, filed November 21, 2012, and published February 2, 2016.
- [S3] N. Cvijetic, G. Milione, E. Ip and T. Wang, *Sci. Rep.*, 2015, **5**, 15422.
- [S4] K. Obata, Gesture Recognition Apparatus, Gesture Recognition Method, and Recording Medium. U.S. Patent 20140153774 A1, filed September 19, 2013, and published June 5, 2016.
- [S5] F. Aezinia, Y. Wang and B. Bahreyni, *IEEE T. Consum. Electr.*, 2012, **58**, 886-890.
- [S6] Y. L. Lee, Linear Capacitance Measurement and Touchless Switch. U.S. Patent 7323886 B2, filed August 12, 2005, and published January 29, 2008.
- [S7] G. Hernandez, Fabry-Pérot Interferometers. *Cambridge: Cambridge University Press*. ISBN 0-521-32238-3 (1986).
- [S8] D. Feuermann, J. M. Gordon and M. Huleihil, *Sol. Energy*, 2002, **72**, 195-204.
- [S9] S. G. Jennings, R. G. Pinnick and J. B. Gillespie, *Appl. Optics*, 1979, **18**, 1368-1371.
- [S10] R. Moghimi, *Analog Dialogue*, 2000, 34-7.